Evaluation of river discharges monitored by a fixed side-looking Doppler profiler

J. Le Coz, G. Pierrefeu, P. Paquier

Evaluation of river discharges monitored by a fixed side-looking Doppler profiler

J. Le Coz,[1] G. Pierrefeu,[2] and A. Paquier[1]

Received 1 March 2008; revised 11 July 2008; accepted 13 August 2008; published 26 November 2008.

[1] Fixed side-looking Doppler current profilers (H-ADCP) recently emerged as an innovating technique for the continuous monitoring of river discharges. The discharge can be computed from the flow velocities measured by the H-ADCP along a horizontal profile across the section. This paper reports a field assessment of the quality of velocities and discharges provided by a 3-narrow-beam Teledyne RD Instruments, Inc. (RDI) 300 kHz H-ADCP installed at the Saint-Georges gauging station (Saône river in Lyon, France). Reference velocity and discharge values were established from 18 conventional ADCP river gauging campaigns over an extended discharge range (100–1800 m^3/s). The comparison with ADCP data revealed that H-ADCP velocity measurements were reliable (deviations <5%) in a near-field range only (60 m out of a 95 m total section width). In the far field (beyond 60 m), H-ADCP velocity measurements showed negative bias of up to −50% 90 m from the instrument. For section-averaged velocities lower than 0.4 m/s approximately, H-ADCP velocity measurements were found to be significantly underestimated over the whole cross section. The performances of several strategies (index velocity method and velocity profile method) for computing discharge were tested, compared, and discussed. For the velocity profile method, several profile laws and far-field extrapolation methods were implemented. Both methods gave acceptable discharge values (deviations <5% typically) excepted at low-flow conditions. The reasons why H-ADCP velocities were unacceptably biased low in the far field and for low flow conditions require further investigation in order to define correcting measures.

Citation: Le Coz, J., G. Pierrefeu, and A. Paquier (2008), Evaluation of river discharges monitored by a fixed side-looking Doppler profiler, *Water Resour. Res.*, *44*, W00D09, doi:10.1029/2008WR006967.

1. Introduction

[2] The real-time monitoring of discharge in natural streams and man-made canals is difficult. It requires both the continuous survey of some hydraulic parameters and the knowledge of their relationships with the stream discharge. The most common method consists of measuring the water level and establishing a stage-discharge relationship (so-called rating curve [e.g., *Schmidt*, 2002]) fitted from a set of discharge measurements. In some cases, the accuracy and stability of the stage-discharge relationship may be improved if the hydraulic control is exerted by a designed hydraulic work (sill, weir, flume, etc.).

[3] Rating curves are subject to a number of limitations. The stage-discharge relationship can vary with time, according to changes in the channel geometry or roughness (vegetation for instance). When the river reach is hydraulically influenced by backwater effects (dams, lake, sea, etc.), a single-parameter rating (stage for example) is impossible to establish. Extra information is therefore necessary, for instance a second water level measurement for water slope gauging stations [*Rantz*, 1982], or flow velocity measurements.

[4] In recent years, several innovative velocity monitoring systems were applied to streamflow monitoring where the total discharge is computed from the cross-sectional bathymetry profile, the water height and velocity measurements in a more or less extended part of the cross section. For streams with stable geometry over time, the bathymetry profile can be measured by conventional means or extracted from gauging data sets and considered as constant. For unstable sections, the difficult assessment of the wetted area may increase the uncertainty associated with discharge outputs, especially during morphogenic events. Among these flow monitoring techniques, the continuous Doppler flowmeters (so-called sewer meters) measure the bulk velocity in the acoustic beam; however, they can be used for small streams or urban networks only because of their very limited range. Emerging noncontact techniques such as large-scale particle image velocimetry (LSPIV) [*Hauet et al.*, 2008] and radar wave scattering [*Costa et al.*, 2006] allow the measurement of the surface flow velocities. The acoustic transit time flowmeters measure the average velocity along one or several horizontal paths across the section. Fixed side-looking Doppler current profilers (H-ADCP) follow the same principle of operation as acoustic Doppler current profilers (ADCP) increasingly used to gauge rivers; they measure the horizontal water velocity profile along a horizontal line across the section.

[1] Hydrology-Hydraulics Research Unit, Cemagref, Lyon, France.
[2] Compagnie Nationale du Rhône, Lyon, France.

0043-1397/08/2008WR006967$09.00

[5] The installation of a transit time flowmeter station usually requires more extensive infrastructure than the installation of a H-ADCP station. Typically, four sensors have to be installed in the river channel below the free surface, instead of one H-ADCP head. Though alleviated thanks to new communication technologies [*Lengricht et al.*, 2007], cabling operations remain more difficult than for a H-ADCP system. The measuring range of transit time flowmeters is much longer (up to 2000 m) than the range of available H-ADCP systems. However, in case of too high concentration in suspended particles, the measurement may be disrupted because of the attenuation of the acoustic signal throughout the whole cross section. Recently, French hydropower producers Compagnie Nationale du Rhône (CNR) (French hydropower company) and Electricité de France (EDF) [*Carré et al.*, 2008] estimated the installation costs to be on average 10–30 k€ for a classical gauging station (based on water level measurements only), and 100–300 k€ for an ultrasonic station (either H-ADCP or transit time). Whereas the installation costs may be 10 times higher for an ultrasonic station, the operating costs are usually quite similar whatever the type of station (in the range of 10–12 k€ per year).

[6] Several strategies are possible for estimating the discharge from a given bathymetry profile, the externally gauged water height, and H-ADCP velocity measurements. Methods requiring numerical flow modeling are not considered in the present study. The index velocity method (IVM) consists of regressing the section-averaged velocity U given by direct discharge measurements against an index velocity [*Rantz*, 1982] built from the simultaneous H-ADCP velocity measurements. This method is very simple but relies on empirical fits. If the distribution of the dimensionless depth-averaged velocity across the section remains constant over the range of hydraulic conditions, a linear correlation may be found. Alternatively, the total discharge can be computed from theoretical vertical velocity profiles made dimensional with the H-ADCP velocity measurements across the section and integrated over the flow depth (velocity profile method, VPM). Discharge estimates are necessary in unmeasured areas in the vicinity of the transducer and beyond the measuring range. The most commonly used theoretical profiles are the power law (equation (1)), the logarithmic law of the wall (equation (2)), or the van Rijn profile (equation (3)) [*Aqua Vision BV*, 2003; *van Rijn*, 1986], i.e., a linear combination of a logarithmic law and a perturbation law derived from the wake law of the wall [*Coles*, 1956]:

$$\frac{u_z}{u_{z_a}} = \left(\frac{z}{z_a}\right)^{1/m} \tag{1}$$

with u_z the velocity at elevation z above the bed, u_{z_a} the velocity at the reference elevation z_a, and m an empirical coefficient linked to the bottom roughness.

$$\frac{u_z}{u_*} = \frac{1}{\kappa} \ln\left(\frac{z}{z_0}\right) \tag{2}$$

with κ the von Kármán constant (0.41), u_* the shear velocity, and z_0 the roughness length, i.e., the elevation above the bed where the velocity is zero.

$$\frac{u_z}{u_{z=h}} = A_1 \ln\left(\frac{z}{z_0}\right) + \left[1 - A_1 \ln\left(\frac{h}{z_0}\right)\right](2\xi^t - \xi^{2t}) \tag{3}$$

with h the water depth, $u_{z=h}$ the surface velocity, $\xi = (z - z_0)/(h - z_0)$, A_1 an empirical coefficient, and t computed so that $u_{z=0.5h}$ is the same for all A_1 values.

[7] Since 2005, several H-ADCP have been installed in French rivers by the hydrometry services of hydropower producers: Rhône river at Lyon-Perrache and Montélimar, Saône river at Lyon–Saint-Georges, Isère river at Romans on behalf of Compagnie Nationale du Rhône (CNR); Rhône river near the Saint-Alban and Tricastin nuclear power plants on behalf of Electricité de France (EDF). Early verification tests consisted of the comparison of discharges provided by the H-ADCP systems (with VPM) with reference discharge measurements. The Saint-Alban H-ADCP yielded unstable discharge series, with deviations from the reference discharge data being often greater than 20% [*Legras*, 2006]. These bad results were mainly attributed to an inappropriate reach: the H-ADCP was installed in a river bend, with very irregular bed. The resulting complex structure of the flow was assumed to deteriorate the velocity measurement and/or the discharge computation. On the opposite, the Saint-Georges H-ADCP yielded good results (deviations in discharge lower than 5%) obtained in the Saône river during floods [*Pierrefeu*, 2006]. At this time, the few underestimated discharges observed for low-flow conditions were not interpreted as a systematic bias, but as isolated problems probably due to inaccurate stream gauging or influence of the operation of the downstream hydraulic structures, at Pierre-Bénite dams.

[8] The investigation of not only discharges but also velocity measurements provided by H-ADCP systems appears necessary to assess their performance, according to environmental conditions and to the chosen discharge computation strategy. This paper reports the methodology and results of the study of the H-ADCP at Saint-Georges gauging station (Saône river in Lyon, France). In section 2, the characteristics of the flow monitoring system by H-ADCP and the reference measurements by ADCP are described. In section 3, the methodology for postprocessing the reference ADCP data is defined and validated. In section 4, both H-ADCP and postprocessed ADCP velocity data are analyzed in order to define discharge computation strategies, according to the observed H-ADCP performance and flow structure. Last, the quality of the discharges yielded by the IVM, the VPM and the edge extrapolation methods are presented and discussed.

[9] In this paper, the results of the comparison of a quantity X with a reference quantity X_{ref} are expressed by the residuals $R(X, X_{\mathrm{ref}})$:

$$R(X,\ X_{\mathrm{ref}}) = (X - X_{\mathrm{ref}})/X_{\mathrm{ref}} \times 100\ (\%) \tag{4}$$

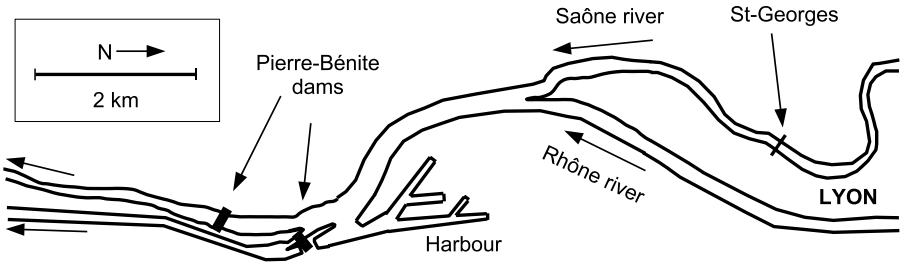

Figure 1. Location map of the study area.

As a general convention, u stands for point velocity; $\langle u \rangle$ for depth-averaged (2Dh) velocity; U for section- or subsection-averaged (1-D) velocity; A for wetted area; Q for discharge.

2. Experimental Setup

2.1. Saint-Georges Gauging Station

[10] The Saône river is the main tributary of the upper French Rhône river. The catchment area is 30,060 km^2 and the average yearly discharge is 442 m^3/s near the confluence with the Rhône river in Lyon [*Astrade and Bravard*, 1999]. A reliable real-time monitoring of discharge supply to the Rhône from the Saône is of paramount importance for flood forecast and hydropower generation. As the last Saône reach is significantly influenced by downstream dams (Figure 1), it is impossible to establish a single-parameter rating curve. Therefore, the discharge is monitored through relationships using the water slope measured between the upstream Couzon gauging station and the Pierre-Bénite dams as a parameter. The Saint-Georges gauging station is located in the right side of a 95 m wide straight reach of the Saône river. The section geometry is trapezoidal, almost symmetric, with a steeper transverse slope in the right side. The water depth is around 10 m at low-flow conditions.

2.2. Side-Looking Doppler Profiler

[11] In February 2006, after several tests in the Saône and Rhône rivers in Lyon, the Compagnie Nationale du Rhône (CNR) equipped the Saint-Georges gauging station with a 3-narrow-beam Teledyne RD Instruments, Inc. (RDI) 300 kHz H-ADCP (Figure 2a). This is a narrow-beam H-ADCP, i.e., with reduced main lobe spreading angle for all transducers (0.7° instead of 3° for previous version).

[12] The H-ADCP sensor is fixed on the right bank in a masonry vertical wall, around 2 m below the usual low-flow water stage, at the elevation 160.00 m above sea level. The three transducers point at −0.58° below the horizontal plane. The heading of the middle beam is 114.5° (derived from the internal compass). Upstream and downstream beams form a 20° angle with the median beam in the horizontal plane (Figure 2b).

[13] Horizontal velocity components are computed from the radial velocity components measured along the three beams by Doppler effect. 180 single ping measurements acquired over 45 s are averaged per minute and recorded by the H-ADCP system. The wetted area A_H is computed from the water level measured by an independent pneumatic pressure gauge (bubbler) and a user-defined bathymetry profile. The water level measurements were checked to be accurate within 5 cm (i.e., the magnitude of the free-surface oscillation) against the direct readings of the staff gauge.

2.3. ADCP Measurement Campaigns

[14] In order to establish reference velocity and discharge data for the evaluation of the H-ADCP performance, 18 ADCP river discharge measurements were performed during a series of floods in February–April 2006 (Figure 3b). The investigated discharge conditions ranged from 100 to 1800 m^3/s. A

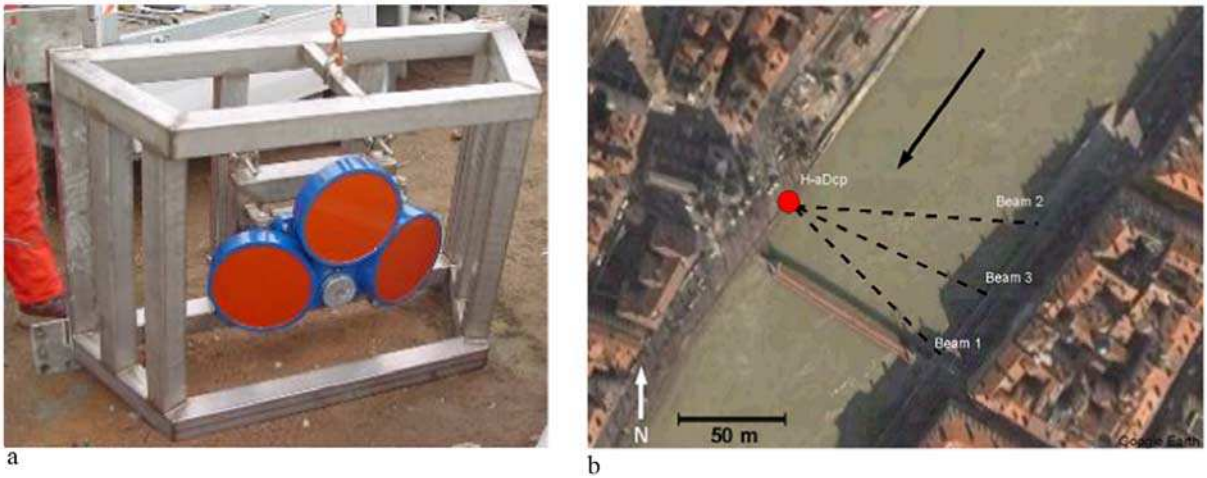

Figure 2. The H-ADCP setup at Saint-Georges gauging station: (a) view of the 3-narrow-beam mount; (b) aerial view of the beam axes across the section (image from Google Earth).

Figure 3. ADCP campaigns at Saint-Georges gauging station: (a) vessel mount; (b) discharge conditions: hydrograph from the Couzon slope-area gauging station, and ADCP gauged discharges Q_0.

summary of the most important hydraulic parameters during the 18 ADCP campaigns at the Saint-Georges gauging station is given in Table 1. The hydraulic conditions remained stationary during the corresponding time span: the ADCP discharge, the H-ADCP mean velocity, the water level recorded by both the operator and the automatic gauge were checked to show no significant variation.

[15] ADCP WorkHorse RioGrande operating at 600 kHz and 1200 kHz were deployed on a bow swing mount with a powered boat (Figure 3a). Water velocities were acquired through the default Teledyne RDI broadband mode 1 (WM1). The velocity bin size (WS) was set to 0.30–0.40 m and measured velocities were 5-ping-averaged (WP5). All data were referenced to the ADCP bottom tracking. Any drift in the bottom tracking due to moving bed effects or compass error was checked, especially for high discharge values: errors in return position after two crossings of the section were not significant. The loop closure test conducted by the hydrometry staff is described by *Le Coz et al.* [2008].

[16] According to the CNR procedures, each gauged discharge value Q_0 was established from a series of 6 (exceptionally 5 or 7) replicate ADCP crossings. Q_0 is the average of the discharges computed by the WinRiver software [*Teledyne RD Instruments*, 2003] for the replicate ADCP crossings. Reported field assessments of the quality of ADCP river discharge measurements usually lead to a widely accepted uncertainty level around 5% [e.g., *Olivier et al.*, 2008; *Oberg and Mueller*, 2007]. However, a rigorous methodology for ADCP discharge uncertainty analysis following available metrological standards is still missing [*Gonzalez-Castro and Muste*, 2007]. In the whole study, Q_0 is the reference ''true'' discharge value.

[17] The bottom tracking data were used to derive ADCP east/north position relatively to the starting point of each transect. All ADCP crossings began from or ended to the H-ADCP position in the right-side embankment, at a distance very close to 1 m. This right shore distance was estimated by eye precisely (error lower than ±0.25 m) from the vertical wall. Starting ADCP transects at an edge distance from a vertical wall less than the water depth may result in corrupted bottom track or water track data because of acoustic interference from the main beam or sidelobes impinging on the wall [*Oberg et al.*, 2005]. However, visual inspection of the bottom track and velocity data in the first ensembles did not yield any sign of decorrelated or biased data. Some sensitivity tests were also performed by subsectioning transects to remove the ensembles situated closer to the edge than the water depth. Changes in the total discharge were insignificant (less than 1% typically).

[18] The elevation of all ADCP data was referenced to the water level through the ADCP transducer depth, precisely measured for each campaign. Data elevation was derived in the French elevation reference system from the staff gauge water level. The frequency difference between ADCP and H-ADCP signals should be high enough to avoid acoustic interference effects in the Doppler analysis performed by both profilers. No suspicious variation in the mean velocity measured by the H-ADCP was observed during the time spans of the ADCP gauging campaigns.

3. Postprocessing of Reference ADCP Data

[19] In order to evaluate the velocities and discharges provided by the H-ADCP system, ADCP data had to be postprocessed to establish the reference bathymetry profile, mean velocity field and 2Dh velocities for each gauging campaign. A methodology for averaging and integrating ADCP data from several replicate crossings was developed and validated [*Le Coz et al.*, 2007b].

Table 1. The 18 Selected ADCP Gauging Series[a]

Code	Date (year/month/day)	Frequency (kHz)	Begin Time, LT	End Time, LT	Q_0 (m^3/s)	R_h (m)	Course (deg)	U_a (m/s)	Froude Fr	Reynolds Re ($\times 10^6$)
SG1	2006/02/15	1200	0948	1002	115	6.96	123.5	0.17	0.02	1.2
SG2	2006/02/16	1200	1410	1425	246	7.06	118.8	0.36	0.04	2.5
SG3	2006/02/16	1200	1644	1657	317	7.04	120.8	0.46	0.05	3.3
SG4	2006/02/17	1200	1030	1049	512	6.88	125.2	0.79	0.10	5.4
SG5	2006/02/18	600	1035	1057	902	7.06	127.4	1.37	0.17	9.6
SG6	2006/02/19	600	1010	1028	1068	7.14	125.7	1.53	0.18	11.0
SG7	2006/02/20	600	0839	0854	1242	7.83	123.3	1.62	0.18	12.7
SG8	2006/02/21	1200	1354	1414	1347	7.87	125.7	1.75	0.20	13.7
SG9	2006/02/22	600	1124	1148	1335	7.55	123.7	1.86	0.22	14.1
SG10	2006/02/27	600	0959	1015	510	7.02	127.6	0.78	0.09	5.5
SG11	2006/03/10	600	0935	0954	1352	7.52	125.2	1.91	0.22	14.4
SG12	2006/03/13	600	1051	1105	1580	7.56	129.9	2.20	0.26	16.6
SG13	2006/03/15	600	1005	1031	1768	7.80	121.0	2.29	0.26	17.9
SG14	2006/03/17	600	0958	1016	1787	7.88	124.0	2.29	0.26	18.1
SG15	2006/03/23	600	1358	1419	692	7.07	123.9	1.04	0.12	7.4
SG16	2006/03/27	600	1045	1117	1035	7.28	121.0	1.45	0.17	10.6
SG17	2006/04/03	600	1124	1143	1552	7.93	132.8	2.05	0.23	16.3
SG18	2006/05/03	600	1035	1135	262	7.07	123.0	0.38	0.04	2.7

[a]The indicated frequency is the operating frequency of the ADCP. The discharge Q_0 and the mean course were established from ADCP gauging campaigns. The hydraulic radius R_h and the section-averaged velocity U_a were computed from the postprocessed ADCP data. The Froude number was computed as $Fr = U_a/\sqrt{g\,D_h}$, with D_h the hydraulic depth computed from the postprocessed ADCP data. The Reynolds number was computed as $Re = U_a R_h/\nu$, with $\nu = 10^{-6}$ m^2/s the kinematic viscosity of water.

3.1. Computation of Reference Bathymetry Profiles and Velocity Fields

[20] For each series, the crossings yielded similar vessel tracks. In particular, the mean length and course values showed dispersion coefficients lower than 3%. The 3-D velocity and bathymetry data were normally projected onto the vertical plane defined by the average course. For each ensemble, the average bed elevation from the four beam measurements was considered. Projected bathymetry profiles are very similar (Figure 4).

[21] For further comparison with H-ADCP data, the projected ADCP data were projected again, along the mean flow direction, and onto the vertical plane defined by the H-ADCP central beam (heading 114.5°). In this plane, averaging node positions were defined to match the H-ADCP sampling positions (every 4 m from 6 m to 94 m from right bank) and the measured ADCP domain (every 0.4 m from the top bin elevation to the sidelobe line, i.e., 6% of water height above the averaged bed level, Figure 4). Thus 414 profiles were obtained (23 verticals for 18 ADCP campaigns).

[22] For each of the 18 ADCP campaigns, the averaged bathymetry was computed as the inverse distance weighting (IDW) average of all neighboring data within 2 m. IDW was used because it is a simple, widely used method, with low computational cost. For each campaign, the interpolated profile was checked to be an accurate average of the projected raw bathymetry profiles. A typical example can be seen in Figure 4.

[23] Similarly, the IDW average of the closest N_i velocity data in a user-defined search surface was affected to each grid node. The fixed number N_i of points to be included in the interpolation was set by the user. If less than N_i velocity data were found in the search surface, the IDW average was not computed. If more than N_i points were found, only the N_i closest points were averaged. Here, the search surface was a 0.8-m-high 2-m-wide rectangle. Consequently search surfaces did not overlap horizontally, but overlapped on half neighboring search surfaces vertically.

3.2. Sensitivity Analysis of the Mean Velocity Field

[24] The resulting vertical velocity profiles were quite smooth as expected for correctly time-averaged velocity data. In the IDW average process used here, an ensemble as well as a spatial averaging allows to reduce velocity data dispersion due to turbulence-induced time fluctuations as well as the Doppler noise linked to the ADCP technology [*Muste et al.*, 2004; *Dinehart and Burau*, 2005].

[25] The sensitivity of the ADCP averaged vertical profiles to N_i was tested. Because of the spatial density of the raw data, for N_i greater than 32, the average velocity could not be computed in a significant number of grid nodes. For each ADCP campaign, two error parameters were computed

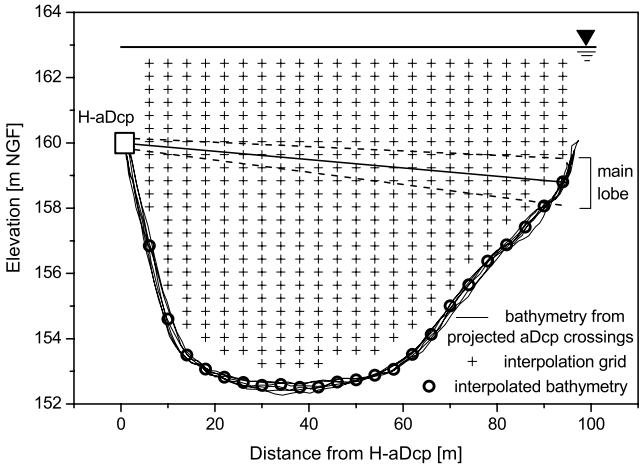

Figure 4. Typical interpolation grid for ADCP data postprocessing (campaign SG12), projected and interpolated bathymetry profiles, and geometry of the H-ADCP main acoustic lobe.

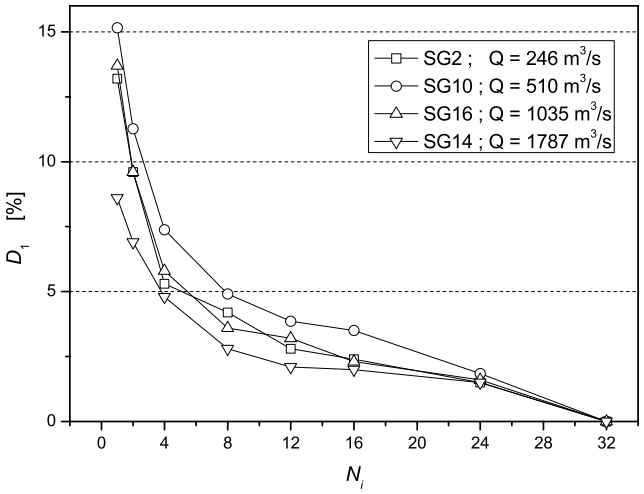

Figure 5. Sensitivity of averaged ADCP vertical profiles to the number N_i of averaged neighboring data: campaign average D_1 of maximum velocity deviations in each vertical profile, for four contrasting discharge values.

from deviations between the averaged vertical profiles computed with a given N_i value, and the corresponding reference profiles computed with $N_i = 32$: D_1 is the mean of the maximum point velocity deviations over all profiles; D_2 is the maximum deviation in the depth-averaged velocity over all profiles.

[26] Figure 5 shows the effect of increasing N_i from 1 to 32 on D_1, for four contrasting discharge values. D_1 is found to be up to 15% for $N_i = 1$ while $D_1 < 5\%$ for $N_i > 8$. D_2 exceeds 25% for $N_i = 1$ whereas $D_2 < 5\%$ for $N_i > 12$. These results are coherent with the detailed examination of typical averaged profiles obtained for varying N_i: for low N_i (1, 2, 4), the averaged profiles are as spiky as the raw "instantaneous" ADCP profiles; for N_i large enough (16, 24, 32), the averaged profiles are in very close agreement to each other, with velocity deviations typically lower than 5%.

[27] N_i was set to 32 for the present study case. As no mean vertical velocity profile acquired by current meter or stationary ADCP deployment was available, the profiles averaged with $N_i = 32$ were taken as the reference true profiles. In practice, such profiles are equivalent to profiles calculated with $N_i = \infty$ but they require much less computational time.

3.3. Velocity Depth Averaging and Discharge Validation

[28] For each postprocessed ADCP vertical velocity profile, the depth-integrated velocity $\langle u_a \rangle$ was computed following the WinRiver1.06 procedure [*Teledyne RD Instruments*, 2003] used in the conventional discharge assessment. The unit discharge was computed as the sum of discharges across vertical bins centered on each grid node, plus discharge estimates for near-surface and near-bed unmeasured zones. The top discharge was estimated with a constant extrapolation, the bed discharge estimate was fitted with a one-sixth power law. Then the depth-integrated velocity was calculated as the unit discharge divided by the water depth. Figure 6 gives a typical horizontal view of the raw and averaged depth-integrated velocities obtained from successive ADCP crossings.

[29] The total postprocessed ADCP discharge Q_a was computed as the sum of the normal component of $\langle u_a \rangle$ multiplied by the space step (4 m) across the averaging transect. Edge discharges were estimated using the equation implemented in WinRiver on the basis of a constant Froude assumption [*Fulford and Sauer*, 1986]. As an evaluation of the ADCP postprocessing procedure accuracy, the 18 resulting discharges Q_a were compared with the corresponding gauged Q_0 discharges. For each campaign, Q_0 is the average of the discharges by WinRiver over the replicate ADCP crossings; Q_a is the discharge computed from the postprocessed ADCP bathymetry and velocity data. Residuals

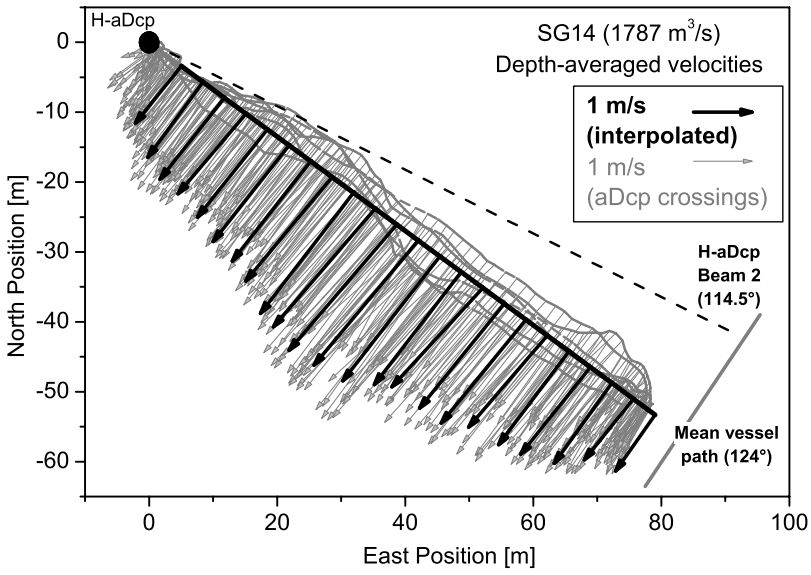

Figure 6. Typical ADCP vessel tracks and depth-averaged velocity fields: raw and averaged data. In the actual postprocessing procedure, raw ADCP data are projected on the H-ADCP central beam axis along the mean flow direction before averaging.

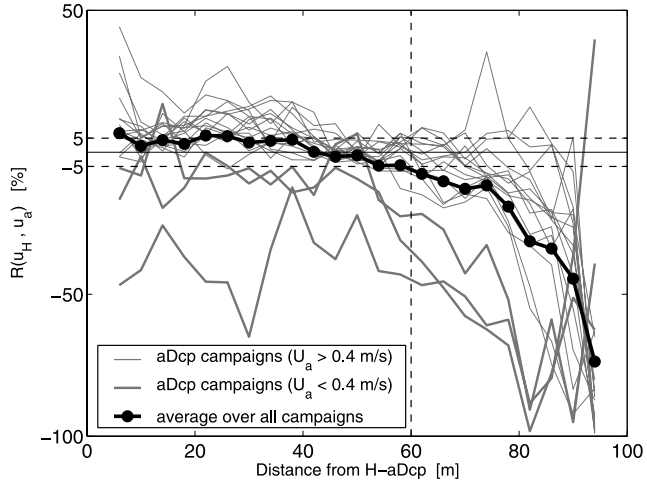

Figure 7. Comparison of point velocities measured by the H-ADCP u_H with corresponding ADCP velocities u_a, for all 18 ADCP gauging campaigns.

$R(Q_a, Q_0)$ were typically lower than 1% and the mean deviation over the 18 series was −0.3%. This bias is not significant. Consequently $\langle u_a \rangle$ was taken as the reference depth-integrated velocity for each vertical profile. For comparisons of discharges and 1-D velocities, the gauged discharge Q_0 and the gauged section-averaged velocity $U_a = Q_0/A_a$ (with A_a the wetted area computed from the postprocessed ADCP bathymetry) were taken as the reference values.

4. Configuration of H-ADCP Discharge Computation Strategies

4.1. Evaluation of H-ADCP Velocity Measurements

[30] On each vertical, 15-min averaged H-ADCP velocity measurements u_H were compared to the corresponding ADCP measurements u_a at the closest elevation. The elevation of H-ADCP bin centers were calculated considering the −0.58° angle that H-ADCP beams form with the horizontal plane (Figure 4). The overlapping of several ADCP grid nodes by H-ADCP sampling volumes due to the H-ADCP beam spreading angle (0.7°) was not taken into account. Some sensitivity tests revealed insignificant differences in the final comparison results.

[31] Figure 7 shows that (1) on average, H-ADCP and ADCP velocity measurements are in acceptable agreement (<5%) up to about 60 m from the H-ADCP sensor; the small deviations may be explained by differences in H-ADCP and ADCP sampling geometries; (2) beyond 60 m, H-ADCP velocities rapidly fall and are unacceptably biased low (about −50% at 90 m); (3) for low flow rates ($Q_0 < 300$ m^3/s or $U_a <$ 0.4 m/s), H-ADCP velocity cross profiles deviate from the mean trend, showing significant underestimation over the whole range. In particular, for the lowest discharge (campaign SG1, $Q_0 = 115$ m^3/s, $U_a = 0.17$ m/s), the mean bias is around −50% over the whole cross section. The filtration of water samples indicated that during the low-flow periods, suspended-load concentrations were as low as 10 mg/L or even less [*Le Coz et al.*, 2007a].

[32] These observations were confirmed by further discharge comparison tests conducted by *Pierrefeu* [2008] on the H-ADCP installed by the CNR in three sections (Saône river at Saint-Georges, Isère river at Romans, Rhône power canal at Montélimar). Further investigation is required to understand the causes for such an underestimation in the far field and at low-flow conditions. Considering the reduced spreading of the main acoustical lobe (0.7°) and the limited section width (95 m), problems due to main lobe reflection from the free surface and from the bed were not expected. But sidelobe reflections might also interfere with the signal backscattered by suspended particles. At low concentration, indeed, the backscatter intensity as well as the sound attenuation rate are low.

[33] The observation of H-ADCP velocity measurements led to the following consequences for establishing discharge computation strategies. For the application of the index velocity method (IVM) as well as the velocity profile method (VPM), H-ADCP velocity data were considered only in the reliable range, from 4 to 60 m from the sensor (verticals $1 \leq j \leq j_0$ with $j_0 = 14$). For the VPM, discharge extrapolation was necessary for a significant part of the cross section (around a third of the wetted area). For the IVM as well as the VPM, some large underestimating biases at low flow conditions ($U_a < 0.4$ m/s) were expected.

4.2. Far-Field Extrapolation Methods

[34] Several strategies for extrapolating VPM discharges beyond the H-ADCP measuring range are possible. Four methods were defined and tested by analyzing the flow structure yielded by postprocessed ADCP data. For each ADCP gauging campaign, depth-averaged velocities $\langle u_a \rangle$ were divided by U_a in order to establish the cross profile of the dimensionless 2Dh velocity (Figure 8). $\langle \overline{u}_a \rangle$ was defined as the average of the dimensionless cross profiles, over all the 18 ADCP campaigns. $\langle \overline{u}_a \rangle$ was representative for the whole discharge range, with most of the individual profiles falling in the 5% interval (Figure 8). As the dimensionless flow structure was conserved, a linear correlation should be found between U_a and the index velocity U_{IV}.

[35] Once made dimensional, the mean cross profile can be used in the VPM to extrapolate the discharge in

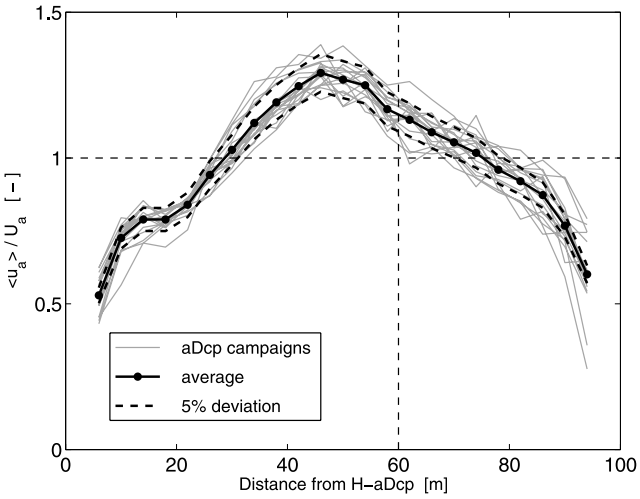

Figure 8. Dimensionless 2Dh ADCP velocity cross profiles for all 18 ADCP gauging campaigns, and average $\langle \overline{u}_a \rangle$.

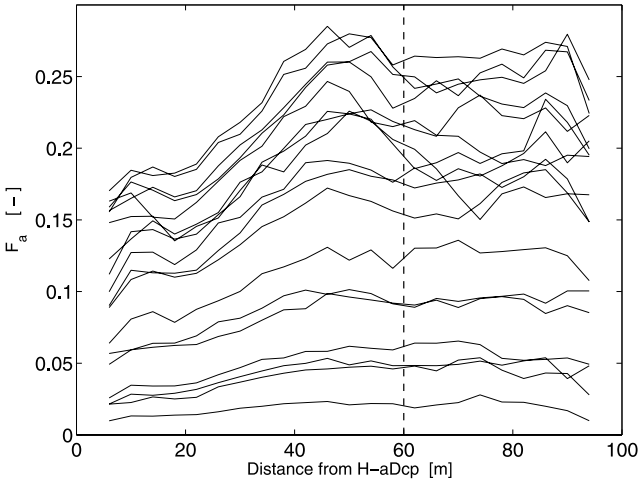

Figure 9. Local Froude numbers $F_a = \langle u_a \rangle / \sqrt{g\ h_a}$ for all 18 ADCP gauging campaigns.

the areas where H-ADCP measurements were discarded ("M extrapolation"):

$$\forall j > j_0 \qquad \left\langle u_j^{\mathrm{M}} \right\rangle = \frac{U_{\mathrm{VPM}}^{\mathrm{nf}}}{\overline{U}_a^{\mathrm{nf}}} \left\langle \overline{u}_{a,j} \right\rangle \tag{5}$$

with $\langle u_j^{\mathrm{M}} \rangle$ the extrapolated depth-averaged velocity at vertical j and $\langle \overline{u}_{a,j} \rangle$ is the dimensionless 2Dh velocity from the mean ADCP cross profile. $\overline{U}_a$ is the 1-D dimensionless velocity computed from $\langle \overline{u}_a \rangle$. $U_{\mathrm{VPM}}^{\mathrm{nf}}$ is the mean velocity over the near-field area (within 60 m) derived from the VPM.

[36] Another extrapolation method can be based on the constant Froude assumption, considering that the ratio of kinetic to potential energy remains constant throughout the cross section. This method is expected to perform correctly for uniform velocity distributions [*Fulford and Sauer*, 1986]. However, a sufficient number of velocity measurement verticals should be used and the validity of the constant Froude assumption should be checked with complete velocity data sets.

[37] The Froude number $F_a = \langle u_a \rangle / \sqrt{g\ h_a}$, with g the acceleration of the gravity, h_a the averaged ADCP water depth, was computed for each vertical throughout the cross section, for all 18 ADCP campaigns (Figure 9). Clearly, the constant Froude assumption is not correct in the half section close to the H-ADCP, where the local Froude number decreases toward the channel side. However, in the farthest half of the section (beyond 50 m), the ratio appears reasonably constant (10% variation typically). Consequently, depth-averaged velocities in discarded verticals may be estimated by ("F extrapolation"):

$$\forall j > j_0 \qquad \left\langle u_j^{\mathrm{F}} \right\rangle = \sqrt{\frac{h_j}{h_{j_0}}} \left\langle u_{\mathrm{VPM},j_0} \right\rangle \tag{6}$$

with $\langle u_j^{\mathrm{F}} \rangle$ the extrapolated depth-averaged velocity at vertical j (local water depth h_j), and $\langle u_{\mathrm{VPM},j_0} \rangle$ the depth-averaged velocity derived by the VPM at the last validated vertical j_0, 60 m from the right bank (local water depth h_{j_0}).

[38] The following "C extrapolation" method consists in extrapolating the last 2Dh velocity in the near field to the rest of the section:

$$\forall j > j_0 \qquad \left\langle u_j^{\mathrm{C}} \right\rangle = \left\langle u_{\mathrm{VPM},j_0} \right\rangle \tag{7}$$

with $\langle u_j^{\mathrm{C}} \rangle$ the extrapolated depth-averaged velocity at vertical j, and previous definition for $\langle u_{\mathrm{VPM},j_0} \rangle$.

[39] A more basic method assumes a constant mean velocity throughout the section. The "U extrapolation" simply consists of applying the VPM-derived mean velocity in the near field to the whole section:

$$U_{\mathrm{VPM}}^{\mathrm{U}} = U_{\mathrm{VPM}}^{\mathrm{nf}} \tag{8}$$

Except for M extrapolation method, the a priori behavior of extrapolation methods can be assessed from direct discharge computation with the mean dimensionless cross profile $\langle \overline{u}_a \rangle$ (Figure 8) and the average ADCP bathymetry. For the considered study site, no significant bias in total discharge (−0.1%) for the F extrapolation method, an underestimating bias (−4%) for the U extrapolation method, and an overestimating bias (+5%) for the C extrapolation method were predicted.

4.3. Assessment of Vertical Profile Laws

[40] For applying the VPM, the analysis of the vertical flow structure yielded by ADCP measurements was helpful for determining a vertical velocity profile law. The average and experimental standard deviation of all the postprocessed ADCP velocity profiles in the near field over the 18 gauging campaigns were computed in 0.04-high layers over the flow depth (Figure 10). Scattering increases near the bed and the free surface but experimental standard deviations remain lower than 0.05 for $0.25 < z/h < 0.90$.

[41] The average dimensionless profile reasonably followed the log law up to $z/h = 0.65$, which corresponds to the core of the outer region of the boundary layer, as observed

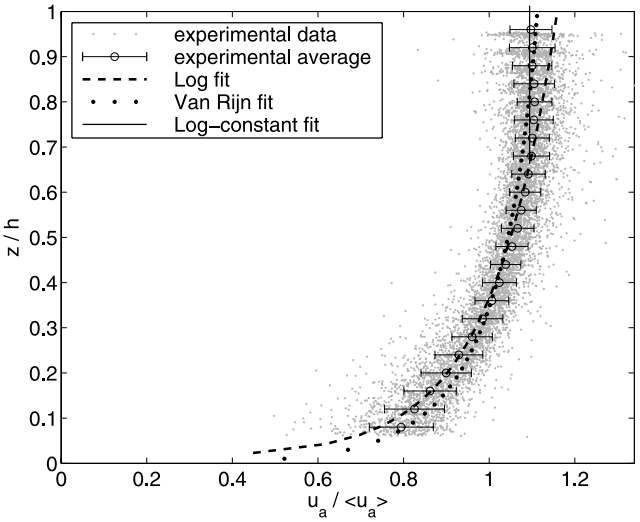

Figure 10. Dimensionless ADCP vertical velocity profiles: data cloud for all profiles in the near field (i.e., from 4 m to 60 m from the H-ADCP), experimental mean and standard deviation, and theoretical fits.

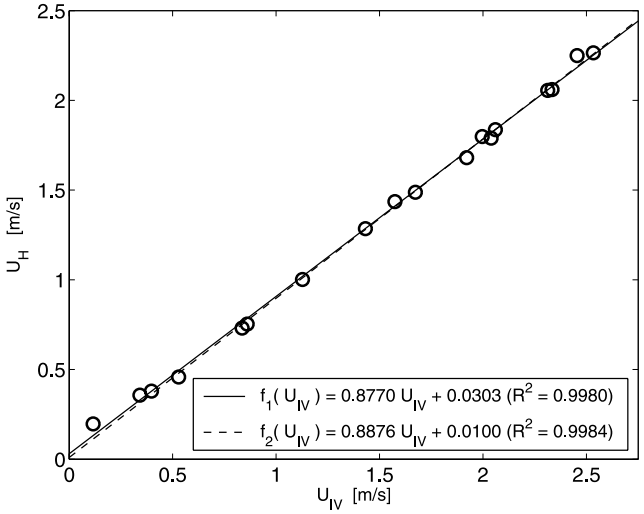

Figure 11. IVM ratings fitted by linear regression over all 18 ADCP campaigns (f_1), and excluding campaign SG1 (f_2).

by *Cardoso et al.* [1989]. For $z/h > 0.65$, the average profile deviated from the log law, probably due to wake or backwater effects due to the dam, and remained constant up to the free surface. Therefore, the log law (equation (2)) as well as the equivalent one-sixth power law (equation (1)) were expected to overestimate flow velocities calculated with the VPM in the present study case.

[42] In addition to these two profile laws, two modified log laws were tested for VPM computation: the van Rijn profile (equation (3)) and the "log constant" profile, i.e., a dimensionless profile following the log law below a given cut level and constant above it.

[43] The parameters of the different laws were chosen as follows. For the log law (Figure 10), $z_0 = 0.0027$ m was estimated from the log fit of the mean ADCP vertical profile over the whole flow depth. As the order of magnitude of z_0/h is 10^{-3}, the equivalent power law corresponded to $m = 6$. For the log constant law (Figure 10), the cut level was set to $z/h = 0.65$ and $z_0 = 0.0057$ m stemmed from the log fit of the mean ADCP vertical profile up to $z/h = 0.65$. For the van Rijn law (Figure 10), $z_0 = 0.0027$ m was retained from the log fit over the whole flow depth; $A_1 = 0.075$ yielded the best fit against the experimental profile (Figure 10). This best van Rijn profile was not as accurate as the log fit for $z/h < 0.65$, but it fell within one experimental standard deviation throughout the whole flow depth.

5. Evaluation of Discharge Computation Methods

[44] The quality of discharge estimates provided by the index velocity method (IVM) and velocity profile method (VPM) was assessed by comparison with the reference ADCP data. In the IVM approach, a rated cross section is used to determine the wetted area for computing the discharge. This bathymetry profile may correspond to a separate location than the measurement section. In the VPM approach, the bathymetry profile of the H-ADCP cross section is required in order to compute vertical velocity profiles and the corresponding discharge.

[45] In this study, both methods were applied using the same user-defined H-ADCP bathymetry profile, which was established as the mean of the postprocessed ADCP bathymetry profiles. Thus, the comparison of mean velocities $U = Q/A_H$, with A_H the wetted area calculated from the H-ADCP bathymetry profile and the measured water level, is equivalent to the comparison of discharges Q. For each gauging campaign, the reference mean velocity in the H-ADCP section writes: $U_H = Q_0/A_H$, with Q_0 the reference discharge, gauged by ADCP.

5.1. Index Velocity Method

[46] Following the index velocity method (IVM), a linear fit of the gauged section-averaged velocity U_H function of an index velocity U_{IV} was performed by a least squares regression technique. U_{IV} was defined as the average of all H-ADCP velocity measurements validated against the corresponding ADCP data, i.e., from 4 m to 60 m from the H-ADCP sensor. From the velocity analysis reported above, a linear correlation $U_H = f(U_{\mathrm{IV}})$ was expected to be accurate excepted for low-flow conditions were H-ADCP velocities were found to be biased low. The corresponding IVM discharge was computed as

$$Q_{\mathrm{IVM}} = f(U_{\mathrm{IV}})A_H \tag{9}$$

[47] The linear regression over all 18 ADCP campaigns (Figure 11) yielded $f_1(U_{\mathrm{IV}}) = 0.8770\ U_{\mathrm{IV}} + 0.0303$ with goodness of fit $R^2 = 0.9980$. As the campaign SG1 (corresponding to the lowest discharge 115 m^3/s) was observed to be an outlier, the regression was also performed excluding SG1, leading to $f_2(U_{\mathrm{IV}}) = 0.8876\ U_{\mathrm{IV}} + 0.0100$ with goodness of fit $R^2 = 0.9984$.

[48] Residuals $R(f_1(U_{\mathrm{IV}}), U_H)$ and $R(f_2(U_{\mathrm{IV}}), U_H)$ for both empirical relationships f_1 and f_2 are presented Figure 12a. As expected from the evaluation of H-ADCP velocity measurements, $f_1(U_{\mathrm{IV}})$ was biased low at low-flow conditions ($U_a < 0.4$ m/s), with unacceptable deviation (−34.1%) for $U_a = 0.17$ m/s (SG1). For $U_a > 0.4$ m/s, residuals were acceptable (mean deviation: +0.6%): they were lower than 5%, excepted for the two campaigns with $U_a \approx 0.8$ m/s (+6.5% for SG10 and +5.3% for SG18). Results for $f_2(U_{\mathrm{IV}})$ were quite similar, but residuals were lower than 5% for all campaigns, excepted for SG1, which showed decreased though still unacceptable underestimation (−15.8%).

[49] Of course, polynomial fits with higher orders can be used to reduce these low-flow residuals. However, using such a high-order relationship to compute discharges may be very dangerous because it not only reflects a hydraulic relationship but also compensates a measuring bias that is not fully understood at present. At least, many repeated low-flow ADCP campaigns for varying suspended sediment concentration should be used to test the validity of the index relationship over the whole range of low-flow measuring conditions.

5.2. Velocity Profile Method in the Near Field

[50] The velocity analysis showed that because of low-biased H-ADCP velocities beyond 60 m, discharges needed to be extrapolated in a large part of the section. Before evaluating the total discharges derived by the VPM, implying the selection of an appropriate far-field extrapolation technique, mean velocities averaged over the near-field

subsection were compared to U_a^{nf} the mean velocity gauged by ADCP in the corresponding subsection. This comparison intended to test the performance of the VPM depending on the selected profile law (and not on the extrapolation method).

[51] The log, power, log constant and van Rijn profile laws and their configurations are reported above (section 4.3). The residuals $R(U_{VPM}^{nf}, U_a^{nf})$ of the corresponding near-field mean velocities against the reference near-field velocities are plotted in Figure 12b.

[52] VPM near-field velocity estimates appeared to be underestimated for the three campaigns with $U_a < 0.4$ m/s, as expected from the H-ADCP velocity analysis. But they were acceptable for $U_a > 0.4$ m/s, though a systematic overestimation was observed for all the four profile laws. The average deviation over the 15 campaigns with $U_a > 0.4$ m/s were +2.4% (log constant), +4.2% (power), +3.3% (log), and +5.6% (van Rijn). Consequently, the log constant theoretical profile appeared as the most recommended law to use for the application of the VPM at the Saint-Georges gauging station. This was to be expected from the ADCP velocity analysis, since the log constant profile was the closest to the mean experimental profile. However, all fitted laws led to velocity estimates affected by a positive bias, likely due to the limitations of the theoretical profiles to represent accurately the mean profile established experimentally from ADCP data.

5.3. Velocity Profile Method With Far-Field Extrapolation

[53] As the log constant configuration yielded the best velocities in the near-field subsection, this profile law was selected for further evaluation of the performance of far-field discharge extrapolation methods. As for the evaluation of IVM results, comparisons of section-averaged velocities $U_{VPM} = Q_{VPM}/A_H$ with the total reference mean velocity U_H are presented hereafter. The M extrapolation (mean ADCP 2Dh profile), F extrapolation (constant Froude), U extrapolation (mean velocity), and C extrapolation (last velocity) methods are defined and discussed in section 4.2.

[54] The residuals of U_{VPM}^{M}, U_{VPM}^{F}, U_{VPM}^{U}, and U_{VPM}^{C} against U_H for all 18 gauging campaigns are plotted Figure 12c. U_{VPM} remained biased low or very low for $U_a < 0.4$ m/s. For $U_a < 0.4$ m/s, the systematic deviation observed for U_{VPM}^{nf} with the log constant law (mean deviation +2.4%) was enhanced or attenuated. The trends were coherent with the a priori assessment of biases expected for the four extrapolation methods (section 4.2). For the M and F extrapolation methods, assumed to be unbiased, the residuals for U_{VPM} (mean deviations +5.6% and +3.6%, respectively) were slightly higher than the residuals previously observed for U_{VPM}^{nf}. The C extrapolation method (expected bias +5%) increased the U_{VPM} velocity overestimation to unacceptable levels (mean deviation +9.3%). On the opposite, the U extrapolation method (expected bias −4%)

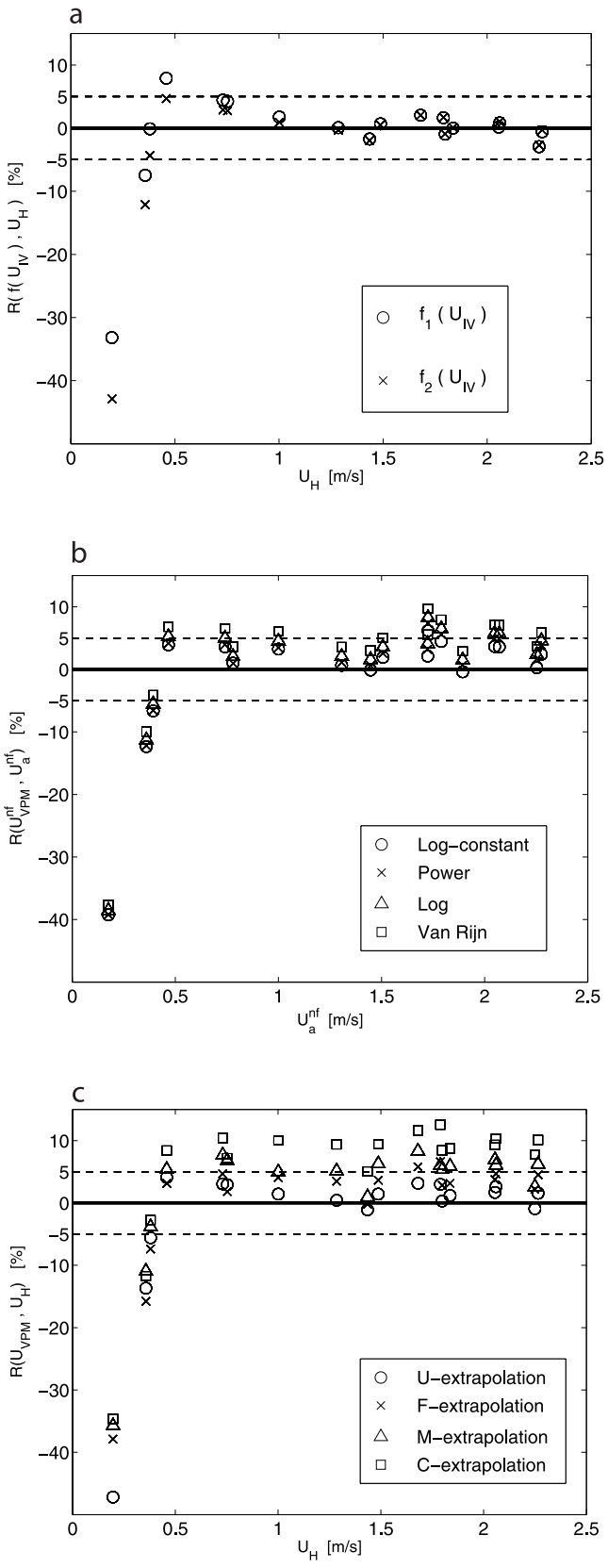

Figure 12. (a) Comparison of the IVM 1-D velocities with the gauged 1-D velocities U_H, for empirical relationships f_1 and f_2; (b) comparison of VPM mean velocities in the near-field subsection U_{VPM}^{nf} with the corresponding ADCP mean velocities U_a^{nf}, for several profile laws; (c) comparison of the VPM section-averaged velocity U_{VPM} with the gauged 1-D velocities U_H, for the log constant profile law and for several extrapolation methods.

compensated the U_{VPM} velocity overestimation (mean deviation +1.7%).

6. Conclusions

[55] Horizontal velocity cross profiles measured by the H-ADCP at Saint-Georges gauging station (Saône river in Lyon, France) were compared to concurrent ADCP measurements for 18 discharge values distributed over the 100–1800 m^3/s range. H-ADCP discharges were computed by the index velocity method (IVM) and the velocity profile method (VPM, with several far-field extrapolation techniques). Once properly postprocessed, the ADCP data were useful for analyzing the mean flow structure, assessing the quality of H-ADCP velocity measurements, and defining reasonable discharge computation methods. Similar analyses can also be conducted with data from velocity-area gauging data sets measured with current meters, for instance.

[56] The comparison with ADCP data revealed that H-ADCP velocity measurements were reliable (deviations <5%) in a near-field range only (60 m out of a 95 m total section width). In the far field (beyond 60 m), H-ADCP velocity measurements showed negative bias of up to −50% 90 m from the instrument. For section-averaged velocities lower than 0.4 m/s approximately, H-ADCP velocity measurements were found to be significantly underestimated over the whole cross section. The main practical conclusions are that (1) avoiding free-surface and bed reflections by considering the main lobe geometry is not a sufficient condition to extend the H-ADCP profiling range; (2) H-ADCP limitations must be taken into account for defining robust discharge computation procedures; and (3) whatever the computation method, discharge estimates are unacceptably biased low under a critical discharge value.

[57] At Saint-Georges gauging station, for $U_a > 0.4$ m/s, both the IVM and VPM gave acceptable discharge values (typically deviations <5%). However, over the 18 available gauging campaigns by ADCP, the H-ADCP section-averaged velocities provided by the IVM were more accurate than those provided by the VPM for any tested configuration, which are overestimated by a few percent (Figure 12). For the application of the VPM, the log constant law and the Froude constant extrapolation method were found to be the most accurate options separately. However, the uniform velocity extrapolation method, with slight underestimating bias, somehow compensated the slightly overestimated near-field velocity computed with the log constant law.

[58] A physically robust method is required for the computation of discharges from H-ADCP velocity measurements, while a limited number of direct discharge measurements over a limited discharge range are available. As an empirical optimization, the IVM is designed to yield the best agreement between H-ADCP outputs and the available control data. Of course, if the VPM theoretical profile was calibrated empirically, the resulting H-ADCP discharges would reach a similar degree of accuracy. The configuration of the VPM parameters on a physical basis requires more sophisticated assumptions on the flow structure than the application of the IVM. However, this study shows how this can be achieved with previously acquired gauging measurements, or with reasonable a priori hydrodynamical assumptions. Both methods require extensive verification tests after installation by stream gauging campaigns over the widest range of hydraulic conditions.

[59] Anyway, in the VPM approach, the physical relevance of the chosen vertical velocity distribution could be checked, whereas the physical relevance of the IVM relationship may be more difficult to assess for a given site. Problems such as instrumental bias or temporary changes in the flow field structure may affect the IVM relationship, even if it remains linear. Therefore the IVM empirical relationship may hide some basic errors that would require a large number of control discharge data to be evidenced and corrected. Following these considerations, the physically based VPM is expected to be more robust, especially for ungauged conditions. The VPM can be seen as a compromise choice between an IVM empirical correlation and hydraulic modeling strategies, which require much more expertise.

[60] The reasons why H-ADCP velocities are unacceptably biased low in the far field and for low velocity and low suspended sediment concentration conditions are still under investigation. Further research work on the H-ADCP backscatter intensity is planned in order to look for methods for discarding/correcting low-biased velocity measurements, and also for converting the backscatter intensity into suspended sediment concentrations, in order to monitor solid fluxes continuously.

Notation

$f(U_{IV})$ IVM 1-D velocity computed from linear regression [LT^{-1}].

$f_1(U_{IV})$ IVM 1-D velocity computed from linear regression over all 18 ADCP campaigns [LT^{-1}].

$f_2(U_{IV})$ IVM 1-D velocity computed from linear regression over all 18 ADCP campaigns excepted SG1 (lowest discharge)[LT^{-1}].

g acceleration of the gravity [LT^{-2}].

h water depth [L].

h_a water depth from the postprocessed ADCP data [L].

h_j water depth at vertical j from the user-defined H-ADCP bathymetry [L].

j index of the vertical across the section ($1 \leq j \leq 23$) [−].

j_0 index of the last vertical in the near field ($j_0 = 14$) [−].

m coefficient in the power law for vertical velocity profiles [−].

t parameter in the van Rijn law for vertical velocity profiles [−].

u_a point velocity from the postprocessed ADCP data [LT^{-1}].

u_H point velocity from H-ADCP measurements [LT^{-1}].

u_z point velocity at elevation z above the bed [LT^{-1}].

u_* shear velocity [LT^{-1}].

$\langle u_a \rangle$ depth-integrated velocity from the postprocessed ADCP data [LT^{-1}].

$\langle \overline{u}_a \rangle$ mean dimensionless depth-integrated velocity from the postprocessed ADCP data [−].

$\langle \overline{u}_{a,j} \rangle$ $\langle \overline{u}_a \rangle$ at vertical j [−].
$\langle u_j^{\mathrm{C}} \rangle$ extrapolated depth-averaged velocity at far-field vertical j with the C extrapolation method [LT^{-1}].
$\langle u_j^{\mathrm{F}} \rangle$ extrapolated depth-averaged velocity at far-field vertical j with the F extrapolation method [LT^{-1}].
$\langle u_j^{\mathrm{M}} \rangle$ extrapolated depth-averaged velocity at far-field vertical j with the M extrapolation method [LT^{-1}].
z elevation above the bed [L].
z_0 roughness length in the log and van Rijn laws for vertical velocity profiles [L].
A_a wetted area computed from the postprocessed ADCP data [L^2].
A_H wetted area computed from the measured water stage and a user-defined H-ADCP bathymetry profile [L^2].
A_1 empirical coefficient in the van Rijn law for vertical velocity profiles [−].
D_1 campaign-averaged maximum velocity deviation in each vertical profile from the postprocessed ADCP data [− %].
D_2 maximum deviation in depth-averaged velocity over all profiles from the postprocessed ADCP data [− %].
D_h hydraulic depth computed from the postprocessed ADCP data [L].
F_a local Froude number computed from the postprocessed ADCP data ($F_a = \langle u_a \rangle / \sqrt{g\ h_a}$) [−].
Fr cross-sectional Froude number computed as $Fr = U_a / \sqrt{g\ D_h}$ [−].
N_i number of neighboring velocity data used in the ADCP data postprocessing procedure [−].
Q_0 reference discharge (average of six replicate ADCP crossings) [$\mathrm{L}^3\mathrm{T}^{-1}$].
Q_a discharge computed from the postprocessed ADCP data [$\mathrm{L}^3\mathrm{T}^{-1}$].
$Q_{\mathrm{VPM}}^{\mathrm{nf}}$ VPM discharge through the near-field subsection [$\mathrm{L}^3\mathrm{T}^{-1}$].
$R(X, X_{\mathrm{ref}})$ residuals of a quantity X against a reference quantity X_{ref} ($R(X, X_{\mathrm{ref}}) = (X - X_{\mathrm{ref}})/X_{\mathrm{ref}} \times 100$) [− %].
R^2 goodness of fit for the IVM linear regression [−].
Re Reynolds number computed as $Re = U_a R_h / \nu$ [−].
R_h hydraulic radius computed from the postprocessed ADCP data [L].
U_a^{nf} mean ADCP velocity over the near-field subsection [LT^{-1}].
U_a 1-D velocity ($U_a = Q_a / A_a$) from the postprocessed ADCP data [LT^{-1}].
$\overline{U}_a$ mean velocity over the whole section computed from the dimensionless average ADCP profile $\langle \overline{u}_a \rangle$ [−].
$\overline{U}_a^{\mathrm{nf}}$ mean velocity over the near-field subsection computed from the dimensionless average ADCP profile $\langle \overline{u}_a \rangle$[−].
U_H 1-D velocity ($U_H = Q_0 / A_H$) from reference discharge and user-defined H-ADCP bathymetry [LT^{-1}].
U_{IV} index velocity (computed as the average of H-ADCP velocities in the near field) [LT^{-1}].
$U_{\mathrm{VPM}}^{\mathrm{nf}}$ mean VPM velocity over the near-field subsection [LT^{-1}].
$U_{\mathrm{VPM}}^{\mathrm{U}}$ mean VPM velocity over the whole section with the U extrapolation method [LT^{-1}].
κ von Kármán constant [−].
ν kinematic viscosity of water [$\mathrm{L}^2\mathrm{T}^{-1}$].
ξ variable used in the van Rijn law for vertical velocity profiles ($\xi = (z - z_0)/(h - z_0)$) [−].

[61] **Acknowledgments.** This work was supported by the Cemagref and the CNR. The operators that produced all the data and information used in this study are gratefully acknowledged: Xavier Martin, Thierry Pantel, Serge Françon, Nicolas Janin, and Jérôme Laurent (CNR) and Guillaume Dramais and Pascal Roger (Cemagref). The authors appreciate the useful and insightful comments of reviewers and the Associate Editor.

References

Aqua Vision BV (2003), VISEA-H manual, Version 2.xx, Utrecht, Netherlands.

Astrade, L., and J.-P. Bravard (1999), Energy gradient and geomorphological processes along a river influenced by neotectonics (the Saône river, France), *Geodin. Acta*, *12*(1), 1–10.

Cardoso, A., W. H. Graf, and G. Gust (1989), Uniform flow in a smooth open channel, *J. Hydraul. Res.*, *27*(5), 603–616.

Carré, C., C. Perret, A. Khaladi, M. Scotti, and G. Pierrefeu (2008), Costs and management strategy of hydrometric observation networks (in French), paper presented at Hydrological Measurements and Uncertainties Conference, Soc. Hydrotech. de Fr., Paris, 1–2 April.

Coles, D. (1956), The law of the wake in the turbulent boundary layer, *J. Fluid Mech.*, *1*, 191–226.

Costa, J. E., R. T. Cheng, F. P. Haeni, N. Melcher, K. R. Spicer, E. Hayes, W. Plant, K. Hayes, C. Teague, and D. Barrick (2006), Use of radars to monitor stream discharge by noncontact methods, *Water Resour. Res.*, *42*, W07422, doi:10.1029/2005WR004430.

Dinehart, R. L., and J. R. Burau (2005), Averaged indicators of secondary flow in repeated acoustic Doppler current profiler crossings of bends, *Water Resour. Res.*, *41*, W09405, doi:10.1029/2005WR004050.

Fulford, J. M., and V. B. Sauer (1986), Comparison of velocity interpolation methods for computing open-channel discharge, *U. S. Geol. Surv. Water Supply Pap.*, *2290*, 139–144.

Gonzalez-Castro, J. A., and M. Muste (2007), Framework for estimating uncertainty of ADCP measurements from a moving boat by standardized uncertainty analysis, *J. Hydraul. Eng.*, *133*(12), 1410–1930.

Hauet, A., A. Kruger, W. F. Krajewski, A. Bradley, M. Muste, and J.-D. Creutin (2008), Experimental system for real-time discharge estimation using an image-based method, *J. Hydrol. Eng.*, *13*(2), 105–110.

Le Coz, J., G. Pierrefeu, J.-F. Brochot, A. Paquier, B. Chastan, and M. Lagouy (2007a), Suspended-load dynamics during floods in the River Saône, France, paper presented at 10th International Symposium on River Sedimentation, M. V. Lomonosov Moscow State Univ., Moscow, Russia.

Le Coz, J., G. Pierrefeu, M. Jodeau, and A. Paquier (2007b), Mean vertical velocity profiles from aDcp river discharge measurement datasets, paper presented at 32nd Congress of IAHR, Int. Assoc. of Hydraul. Eng. and Res., Venice, Italy.

Le Coz, J., G. Pierrefeu, G. Saysset, J.-F. Brochot, and P. Marchand (2008), *Hydrological Measurements by Doppler Profiler (ADCP)—Practical Guide* (in French), 155 pp., Editions Quae, Paris.

Legras, D. (2006), Setting up of a 300 kHz narrowbeam H-ADCP upstream Saint Alban nuclear power plant on the Rhône river, paper presented at ADCPs in Action, Teledyne RDI, Cannes, France, 7–9 June.

Lengricht, J., G. Stephan, and W. Frey (2007), Venice lagoon monitoring with wireless acoustic transit time flowmeters synced by GPS and Bluetooth, paper presented at 32nd Congress of IAHR, Int. Assoc. of Hydraul. Eng. and Res., Venice, Italy.

Muste, M., K. Yu, and M. Spasojevic (2004), Practical aspects of ADCP data use for quantification of mean river flow characteristics; part I: Moving-vessel measurements, *Flow Meas. Instrument.*, *15*(1), 1–16.

Oberg, K., S. Morlock, and W. Caldwell (2005), Quality-assurance plan for discharge measurements using acoustic Doppler current profilers, *U.S. Geol. Surv. Sci. Invest. Rep.*, *2005-5183*, 35 pp.

Oberg, K. A., and D. S. Mueller (2007), Validation of streamflow measurements made with Acoustic Doppler Current Profilers, *J. Hydraul. Eng.*, *133*(12), 1421–1432.

Olivier, A., B. Blanquart, G. Pierrefeu, and M. Scotti (2008), Uncertainty associated with ADCP-gauged discharges, paper presented at Hydrological Measurements and Uncertainties Conference, Soc. Hydrotech. de Fr., Paris, 1–2 April.

Pierrefeu, G. (2006), Monitoring the Saône river discharge in Lyon by H-ADCP, paper presented at ADCPs in Action, Teledyne RDI, Cannes, France, 7–9 June.

Pierrefeu, G. (2008), Evaluation of the H-ADCP stations of the CNR (in French), technical report, 8 pp., Compagnie Natl. du Rhône, Lyon, France.

Rantz, S. E. (1982), Measurement and computation of streamflow, vol. 2, Computation of discharge, *U.S. Geol. Surv. Water Supply Pap.*, *2175*, 373 pp.

Schmidt, A. R. (2002), Analysis of stage-discharge relations for open-channel flows and their associated uncertainties, Ph.D. thesis, 329 pp., Univ. of Ill. at Urbana-Champaign, Urbana.

Teledyne RD Instruments (2003), WinRiver user's guide, international version (January 2003), Poway, Calif.

Van Rijn, L. (1986), Mathematical modeling of suspended sediment in non uniform flows, *J. Hydraul. Eng.*, *112*(6), 433–455.

J. Le Coz and A. Paquier, Hydrology-Hydraulics Research Unit, Cemagref, 3 bis quai Chauveau CP 220, F-69336 Lyon CEDEX 09, France. (jerome.lecoz@cemagref.fr; andre.paquier@cemagref.fr)

G. Pierrefeu, Compagnie Nationale du Rhône, 4 rue de Châlon-sur-Saône, F-69007 Lyon, France. (g.pierrefeu@cnr.tm.fr)